Characterization of cobalt ferrite-supported activated carbon for removal of chromium and lead ions from tannery wastewater via adsorption equilibrium

Muibat Diekola Yahya [a], Kehinde Shola Obayomi [b,*], Mohammed Bello Abdulkadir [a], Yahaya Ahmed Iyaka [c], Adeola Grace Olugbenga [a]

[a] *Department of Chemical Engineering, Federal University of Technology, Minna, P. M. B. 65, Nigeria*
[b] *Department of Chemical Engineering, Landmark University, Omu-Aran, P. M. B. 1001, Nigeria*
[c] *Department of Chemistry, Federal University of Technology, Minna, P. M. B. 65, Nigeria*

Abstract

In this experiment, cobalt ferrite-supported activated carbon (CF-AC) was developed and characterized via the wet impregnation method for the removal of Cr and Pb(II) ions from tannery wastewater. Batch adsorption was carried out to evaluate the effect of experimental operating conditions (pH of solution, contact time, adsorbent dose, and temperature), and the removal efficiencies of Cr and Pb(II) ions by the developed adsorbents were calculated and recorded for all experimental conditions. These variables were estimated and reported as removal efficiencies of 98.2% for Cr and 96.4% for Pb(II) ions at the optimal conditions of 5, 0.8 g, 80 min, and 333 K for pH, adsorbent dose, contact time, and temperature, respectively. The equilibrium for the sorption of Cr and Pb(II) ions was studied using four widely used isotherm models (the Langmuir, Freundlich, Dubinin-Radushkevich, and Temkin isotherm models). It was found that the Freundlich isotherm model fit better with the coefficient of determination (R^2) of 0.948 4 and a small sum of square error of 0.000 6. The maximum adsorption capacities (Q_m) of Pb(II) and Cr adsorbed onto CF-AC were determined to be 6.27 and 23.6 mg/g, respectively. The adsorption process conformed well to pseudo-second order kinetics as revealed by the high R^2 values obtained for both metals. The thermodynamic parameters showed that adsorption of Cr and Pb(II) ions onto CF-AC was spontaneous, feasible, and endothermic under the studied conditions. The mean adsorption energy (E) values revealed that the adsorption mechanism of Cr and Pb(II) by CF-AC is physical in nature. The results of the study showed that adsorbent developed from CF-AC can be efficiently used as an environmentally friendly alternative adsorbent, for removal of Cr and Pb(II) ions in tannery wastewater.
© 2020 Hohai University. Production and hosting by Elsevier B.V. This is an open access article under the CC BY-NC-ND license (http://creativecommons.org/licenses/by-nc-nd/4.0/).

Keywords: Almond husk; Cobalt ferrite; Equilibrium study; Heavy metals; Adsorption; Removal efficiency

1. Introduction

Industrial wastewater from several industries, such as leather tanning, glass production, dyes and pigments, metal coating, mining activities, and battery manufacture, contains heavy metals (Manjuladevi and Sri, 2017; Czikkely et al., 2018). Wastewater generated from tanneries is heavily contaminated and has high organic and inorganic loads (Lofrano et al., 2013). Organic contents are generated owing to the existence of hair, fertilizer, soluble protein, flesh, and blood particles (Obayomi and Auta, 2019), while inorganic matters are primarily due to the presence of the chromium salt utilized as a tanning agent, sulfide salts, and lime. In industrial wastewater, heavy metals such as Pb, Cd, Cr, Zn, Cu, and Fe, are not biodegradable, and their presence in lakes and streams contributes to bioaccumulation in living organisms (Manjuladevi and Sri, 2017; Czikkely et al., 2018; Wambu et al., 2018). Chromium is abundant in the earth's crust and is commonly utilized in galvanizing tanneries, steel finishing,

and chromate preparation (Yahya et al., 2020a). This occurs in two stable states of oxidation, namely, Cr(III) and Cr(VI). Cr(VI) is of particular concern because of its extreme harmfulness, which could have various adverse effects on the well-being of humans, such as epigastric pain, hemorrhaging, skin contact dermatitis, ulceration, lung malignancy, and tissue necrosis (Swathi et al., 2014; Yahya et al., 2020b). However, this adsorption study is focused on the removal of the total chromium.

Lead is usually found in batteries, pigment printing, manufacturing, photographic materials, and manufacturing explosives. Its health impacts include kidney damage, reproductive system damage, mental disorder, liver damage, and nervous system damage (Singh et al., 2017). Therefore, it is essential to remove Cr and Pb(II) ions from industrial wastewater before releasing them into water body (Huang et al., 2017).

Previous studies have shown that although industrial tannery effluent contains other heavy metals (Cu, Cr, Pb, Fe, and Zn) with high concentrations far above the World Health Organization (WHO) standards as reported by Yakubu et al. (2018), it is discarded into the environment with no treatment. The treatment of tannery effluent using groundnut shell has been investigated by Kothai et al. (2019), and studies have shown that the wastewater is extremely complex and often categorized by contents of organic and inorganic compounds, such as Cr, Ni, Pb, Cd, and Cu. Furthermore, Ali et al. (2019) studied the removal of Pb(II) and Cr ions from aqueous solutions via acid activated carbon prepared from the leaves of *Juniperus procera*, while Yahya et al. (2020b) used raw almond shells in a fixed bed to simultaneously remove Cr and Cu(II) under continuous flow sorption. Both researchers found that the processes were effective and efficient (Singh et al., 2017). However, this study intends to use cobalt ferrite-supported activated carbon (CF-AC) for improved removal of heavy metals.

Various techniques that have been used, at the industrial scale, for the decontamination of toxic metals from wastewater include ion exchange (Srivastava et al., 2010), reverse osmosis (Amarasinghe and Williams, 2007), chemical precipitation (Veit et al., 2005), ultra-filtration (Haktanır et al., 2017), flocculation (Obayomi et al., 2020), and nano-filtration (Chukwu et al., 2017). Nevertheless, these techniques suffer drawbacks such as high operational cost, high maintenance cost, high energy requirements, and non-biodegradability, thus limiting their applicability (Chukwu et al., 2017). Consequently, the search for cheap and cost-effective methods for wastewater treatment is increasingly gaining attention.

The bio-sorption technique is an emerging technology that utilizes low-cost materials such as agricultural wastes including wool, coconut husks, and peat moss (Ahalya et al., 2003; Sharma et al., 2013; Saranya et al., 2016). The use of agricultural wastes like kola-nut testa (Bhatnagar et al., 2015), almond shells (Taha et al., 2018; Yahya et al., 2020b), almond green hull powder (Nasseh et al., 2016), and bean husks (Chukwu et al., 2017), as bio-sorbent materials for heavy metal aqueous solution removal can be attributed to their chemical properties. Studies have revealed that almond husk- and shell-based materials can be activated by several approaches to synthesized activated carbons. This can be synthesized via three different methods: chemical, physical, and physicochemical activation processes. The activation processes lead to production of activated carbon with a large surface area, high porosity, and large pore volume (Taha et al., 2018).

Recently, the application of nano-sized magnetic materials as suitable adsorbents, has gained substantial interests based on their optimum magnetic properties and surface area. This leads to a high removal rate of contaminants, good adsorption efficiency, and rapid separation of adsorbent from solution through magnetic fields (Vazquez-Olmos et al., 2016). Among other nano-sized magnetic materials, the cobalt ferrite material has received wide-ranging attention for toxic metal removal from polluted wastewater due to its distinguished good coercivity, reasonable saturation magnetization, large magneto crystalline anisotropy, mechanical hardness, and chemical stability (Sonja et al., 2019). Since the application of nanoparticles as magnetic materials on some parameters depends on particle size, surface area, morphology, and magnetic material properties (Sonja et al., 2019), the ability to adjust the characteristics of materials is a required feature for the synthesis method. The application of CF-AC adsorbent, for removal of chromium and lead ions from tannery wastewater, has not frequently been addressed in the literature.

In this study, activated carbon was first produced from almond husks and later CF-AC was synthesized via the wet impregnation method. The synthesized adsorbent was characterized by Fourier transform infrared spectroscopy (FTIR), X-ray diffraction (XRD), and scanning electron microscopy with energy dispersive X-ray (SEM/EDX) analyses, and the adsorptive properties were tested on the removal of Cr and Pb(II) ions from the tannery wastewater. The batch adsorption process was adopted, and the kinetic, thermodynamic, and isotherm behaviors were studied.

2. Materials and methods

2.1. Materials

The cobalt nitrate, iron nitrate, and potassium hydroxide, purchased from Panlac Ltd., had a purity of 98%−99%. All the chemicals were of analytical grade. Other materials were almond fruits, a pH meter, an industrial oven, and an Ohaus digital weighing balance.

2.2. Preparation of activated carbon from almond husk

Activated carbon from almond husks was produced through a one-step chemical activation process using potassium hydroxide (KOH) as the activating agent. Tropical almond fruits from Minna were locally sourced, and the husks were extracted, washed, and dried in an oven at 110°C overnight. 50 g of the dried almond husks were then impregnated with KOH at 1:2 ratio to the activating agent (Song et al., 2013). The mixture was properly stirred, allowed to impregnate for 6 h, and then dried at 115°C for 3 h. The dried impregnated samples were then activated at 700°C for 1 h and 20 min. The

obtained samples were then washed repeatedly with distilled water until the pH of the solution was 7.2. Afterwards, the samples were dried at 105°C for 4 h to evaporate any present moisture. The dried samples were milled with the aid of a pestle and mortal, and then sieved in the mesh in the range between 250 μm and 200 μm, to increase their surface area. The resulting samples were kept for further use and analysis.

2.3. Synthesis of CF-AC

The cobalt ferrite-activated carbon (CoFe$_2$O$_4$-AC) was synthesized by the wet impregnation method in an alkaline solution. 0.1 mol Fe(NO$_3$)$_3$·9H$_2$O and 0.05 mol Co(NO$_3$)$_2$·6H$_2$O (98.99% pure JHD) were dissolved in a minimum amount of water at room temperature. The stoichiometric ratio of iron nitrate to cobalt nitrate was 2:1, and 50 g of the prepared activated carbon was added to the solution. The mixed solutions were stirred for several hours and then allowed to age overnight. The formed black gel was dried at 120°C for 6 h to remove moisture content. The obtained dried product was later carbonized at 400°C for 1 h, and then stored for analysis and further use (Yahya et al., 2012).

2.4. Collection of tannery wastewater sample

The wastewater samples were collected from the tanyard of a tannery industry at the Challawa Industrial Area of Kano State, in Nigeria, into a corked amber bottle and kept in a refrigerator until the sample was ready for analysis. The initial concentrations of chromium and lead ions in the collected wastewater were determined using an atomic absorption spectrometer (AAS). The analysis of the tannery wastewater showed high concentrations of Cr(IV) and Pb(II) ions at 2.845 7 and 0.849 2 mg/L, respectively, which are above the permissible limits of WHO and Standard Organization of Nigeria (SON).

2.5. Proximate analysis and adsorbent characterization

The proximate analysis of the synthesized CF-AC, from almond husks, was carried out in accordance with the American Society for Testing and Materials (ASTM) standard methods reported by Ekpete and Horsfall (2011) and Dada et al. (2012). The analyzed parameters included moisture content, ash content, bulk density, pH, volatile matter, and fixed carbon. The functional groups, surface morphology, and surface properties of the activated carbon and CF-AC were performed with FTIR (Perkin-Elmer, Shimadzu FTIR-8400S), SEM (Philips, CM20FEG), and XRD (Philips, PW1800), respectively. The pH measurements were conducted with the British Drug House (BDH) indicator.

2.6. Batch adsorption studies

In a typical batch adsorption study, 0.1 g of CF-AC (adsorbent) was placed in a 250-mL Erlenmeyer flask containing 100 mL of the tannery wastewater (adsorbate) initial concentration. At the initial pH of the adsorbate solution, the flask was swirled for perfect contact between the adsorbent and the adsorbate. Subsequently, it was placed in an isothermal shaker at 30°C at a shaker speed of 200 rpm for 2 h until equilibrium was attained. Prior to equilibrium conditions, the residual Cr and Pb(II) concentrations, at specified time intervals, were taken, filtered, and measured with the aid of atomic absorption spectroscopy (PinAACLE 900Z, USA). The amounts of the adsorbed chromium and lead ions onto the prepared adsorbent and their removal efficiencies were determined using Eqs. (1) and (2):

$$q_e = \frac{V(C_0 - C_e)}{W} \tag{1}$$

$$e = \frac{C_0 - C_f}{C_0} \times 100\% \tag{2}$$

where C_0 is the initial adsorbate concentration (mg/L), C_e is the concentration of the adsorbate at equilibrium (mg/L), C_f is the final adsorbate concentration after the adsorption process (mg/L), V is the volume of the adsorbate (L), W is the mass of adsorbent (mg), e is the removal efficiency, and q_e is the amount of adsorbed metal (mg/g).

3. Results and discussion

3.1. Proximate analysis

The results of the proximate analysis of the synthesized CF-AC from almond husks are shown in Table 1.

From the results of proximate analysis, the moisture content of 3.40% is within the range for Indian Standard Institution (ISI) standards for adsorbents of 1%−6%. The high ash content signifies the level of minerals presented in the samples. The fixed carbon of CF-AC has a high value of 54.70%. The higher the fixed carbon value, the better the quality of the adsorbent becomes. This is because the amount of fixed carbon acts as a main generator of heat combustion. Other properties of the adsorbent such as a pH value of 6.94, a bulk density of 0.37 g/cm^3, and a volatile matter value of 27.95, fall within the ranges of those reported by Dada et al. (2012) and Mierzwa-Hersztek et al. (2019).

3.2. Characterization of developed activated carbon and CF-AC

3.2.1. SEM/EDX result

The properties of the developed adsorbents were characterized to examine the surface properties, which informed the

Table 1
Properties of CF-AC.

Property	Result
Moisture content (%)	3.40
Ash content (%)	13.95
Bulk density (g/cm^3)	0.37
pH	6.94
Fixed carbon (%)	54.70
Volatile matter (%)	27.95

adsorptive characteristics of the adsorbent. Fig. 1(a) and (b) shows the SEM micrographs of the developed activated carbon and CF-AC before adsorption. Fig. 1(c) depicts the SEM micrograph of the developed CF-AC after sorption.

In Fig. 1(a), the surface morphology of the activated carbon that was produced from almond husks depicts the formation of an irregular shaped material, with a little formation of cloud-like materials on the surface of the adsorbent. This could result from the oxidation process occurring on the adsorbent surface during the calcination process. It also shows that the adsorbent has a few pores, cavities, and a relatively smooth and rough surface. As shown in Fig. 1(b), the formations of clear and pristine natural particles were formed when $CoFe_2O_4$ was incorporated into the bulk of the adsorbent. The introduction of cobalt ferrite suggests a considerable degree of ferrite particles, owing to its magnetic nature and the union of a few particles held together by weak surface interaction. It demonstrates that the surface morphology of the adsorbent is porous in nature. The obtained morphology is similar to that reported by Kurian et al. (2015), who found improved surface modification. The entrapment of the accumulated Cr and Pb(II) after the adsorption process is depicted in Fig. 1(c). It shows the adsorption and presence of the heavy metal ions within the adsorbent.

Tables 2 and 3 summarize the CF-AC spectra via the energy dispersive X-ray spectroscopy (EDX) before and after adsorption and confirm the present elements and their weight percentage. The chemical composition of adsorbent samples was analyzed with EDX. Table 2 shows the results of EDX for $CoFe_2O_4$-AC (before adsorption), which indicates the presence of various elements. However, Table 3 indicates the presence of Cr and Pb, which were not present in EDX before adsorption (see Table 2). This shows that Cr and Pb(II) ions were adsorbed onto the surface of the adsorbent.

3.2.2. FTIR spectra of developed adsorbent

FTIR analyses were performed to examine the surface functional group present on the surfaces of the developed adsorbent. Fig. 2(a) shows the FTIR spectra for the activated carbon, Fig. 2(b) demonstrates the CF-AC adsorbent before adsorption, and Fig. 2(c) shows the CF-AC adsorbent after adsorption.

The FTIR spectra of unloaded activated carbon and $CoFe_2O_4$-AC showed several distinct and sharp adsorption bands in

Table 2
EDX elemental composition for CF-AC before adsorption.

Element number	Element symbol	Element name	Atomic content (%)	Weight percentage (%)
6	C	Carbon	64.68	35.57
8	O	Oxygen	5.78	4.24
11	Na	Sodium	7.14	7.51
17	Cl	Chlorine	9.75	15.83
20	Ca	Calcium	0.56	1.03
22	Ti	Titanium	0.10	0.23
26	Fe	Iron	1.03	2.64
27	Co	Cobalt	2.74	7.40
29	Cu	Copper	0.39	1.14
30	Zn	Zinc	7.38	22.08
49	In	Indium	0.44	2.33

different wavelengths. However, the FTIR spectra of the loaded $CoFe_2O_4$-AC adsorbent depicted some shifts in several characteristic bands. The spectrum change indicated a change in the functional groups of the adsorbent after adsorption of Cr and Pb(II) ions. Table 4 depicts the peak assignment presented on the surfaces of the adsorbent materials. This shows the various adsorption bands presented on the produced adsorbents.

The presence of a −OH bound was generally observed in both adsorbents. The small fingerprint peaks of $3\,309.90$ cm^{-1} indicate the formation of a −OH stretch of alcohol, and phenols is linked to the presence of moisture in the materials. Nevertheless, the peak at $2\,931.90$ cm^{-1} indicates the presence of −CH stretching of aliphatic hydrocarbon in the developed CF-AC, and the $1\,643.40$ cm^{-1} peak indicates a −C$=$O stretch of ketones and carboxyl groups. The absence of this peak on the surface of the activated carbon could be a result of the formation of amorphous materials that cover the surfaces of the activated carbon after calcination process. The presence of the carboxyl group was highly observable and noticeable at the adsorption band of $1\,643.40$ cm^{-1} throughout the adsorbent, which could be caused by lignin and hemicellulose. The peak of $1\,535.30$ cm^{-1} could be linked to a −C$=$C stretch of an aromatic ring (Coskun et al., 2018). The peak of $1\,342.50$ cm^{-1} shows a −CH bending vibration, and that of $1\,165.04$ cm^{-1} indicates an S−O effect. It reveals the conversion of ester to carboxylic acid (Yahya et al., 2020c). According to Joshi and Pokharel (2014), a peak of 972.20 cm^{-1} indicates −CH groups that are out of the plane. The comparison of FTIR spectra before and after contact with

(a) Activated carbon before adsorption

(b) CF-AC before adsorption
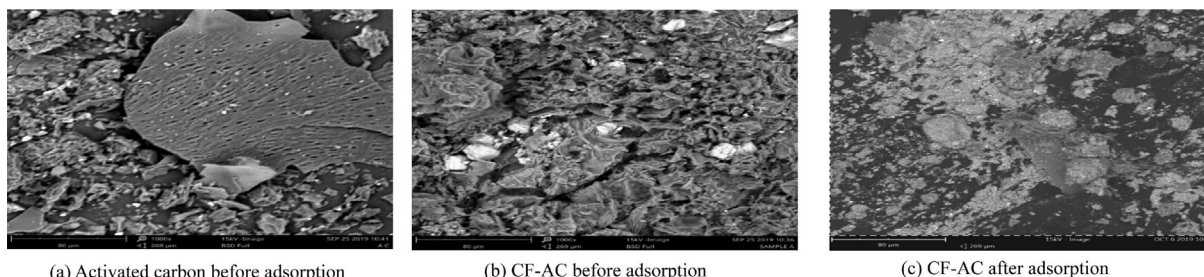
(c) CF-AC after adsorption

Fig. 1. SEM micrographs for activated carbon, CF-AC before adsorption, and CF-AC after adsorption.

Table 3
EDX elemental composition for CF-AC after adsorption.

Element number	Element symbol	Element name	Atomic content (%)	Weight percentage (%)
6	C	Carbon	65.97	35.49
7	N	Nitrogen	1.52	0.96
8	O	Oxygen	9.04	6.48
12	Mg	Magnesium	0.53	0.58
13	Al	Aluminium	0.68	0.82
17	Cl	Chlorine	7.36	11.69
20	Ca	Calcium	0.51	0.91
24	Cr	Chromium	0.42	0.97
26	Fe	Iron	1.52	3.82
27	Co	Cobalt	6.25	16.49
30	Zn	Zinc	5.29	15.50
46	Pd	Palladium	0.32	1.52
53	I	Iodine	0.19	1.08
82	Pb	Lead	0.40	3.71

chromium and lead demonstrates that the peaks attributed to the functional groups presented in the CF-AC significantly decreased after being used as an adsorbent. This indicates the interaction between functional groups and chromium and lead in the solution and demonstrates the role of chemical interactions in adsorption.

3.2.3. XRD spectral of developed adsorbents

The crystallinity of the $CoFe_2O_4$-supported activated carbon adsorbents was determined via the XRD technique and the results are depicted in Fig. 3.
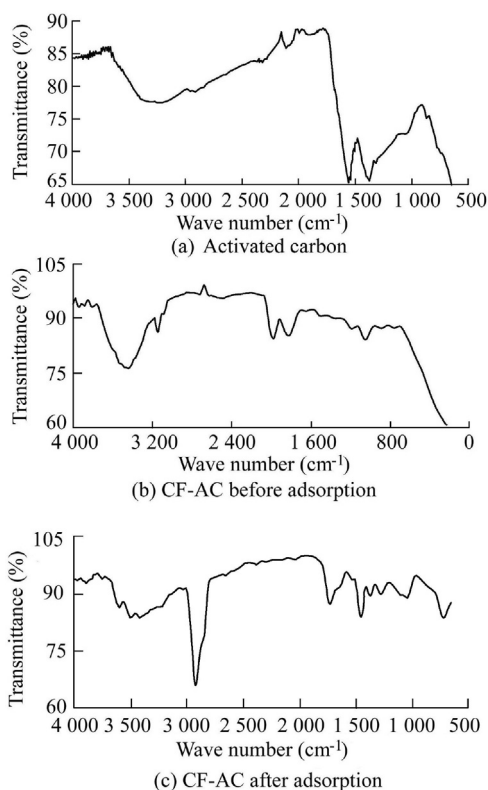

Fig. 2. FTIR spectra of developed activated carbon, CF-AC adsorbent before adsorption, and CF-AC adsorbent after adsorption.

Table 4
FTIR peak assignment of developed activated carbon and CF-AC adsorbents.

Peak (cm^{-1})	Functional group	Vibration type
3 309.90	−OH	Stretching vibration
2 931.90	−CH	Stretching vibration
1 643.40	−C=O	Stretching vibration
1 535.30	−C=C	Stretching vibration
1 342.50	−CH	Bending vibration
1 165.04	S−O	Bending vibration
972.20	−CH	Out of plane

The crystallinity of the developed material illustrated in Fig. 3 shows the presence of several peaks at varied diffraction angles (2θ). The presence of carbon was observed at two different diffraction angles: 23.1° and 43.2°. This is a characteristic peak of carbon materials. The peak formation of the carbon materials was found to be wide, and the width indicates the amorphous nature of the produced particles. The peaks at 26.8°, 44.1°, 56.0°, and 65.4° are attributed to the presence of CoFe metallic phase on the adsorbent surface. These peak formations are in agreement with the findings reported by Cotica et al. (2014).

3.2.4. Brunner-Emmett-Teller (BET) surface area of developed adsorbents

The surface areas of the developed adsorbent were determined via BET, and the results obtained for activated carbon were a surface area of 965 m^2/g, a pore size of 2.24 nm, and a pore volume of 0.44 cm^3/g whereas that of CF-AC were a surface area of 1 098 m^2/g, a pore size of 2.83 nm, and a pore volume of 0.31 cm^3/g. The pore volume of the developed CF-AC was found to be reduced in comparison with that of the initial activated carbon. The reduction in the pore volume could be a result of the incorporation of cobalt ferrite into the bulk of the activated carbon.

3.3. Effect of contact time

Fig. 4(a) represents the effect of contact time on the adsorption efficiency of the $CoFe_2O_4$-supported activated carbon. As shown in Fig. 4(a), the removal efficiency of chromium and lead were observed to increase gradually at the initial stage of the sorption process. The purpose of this could be linked to the fact that the adsorbent at the initial stage
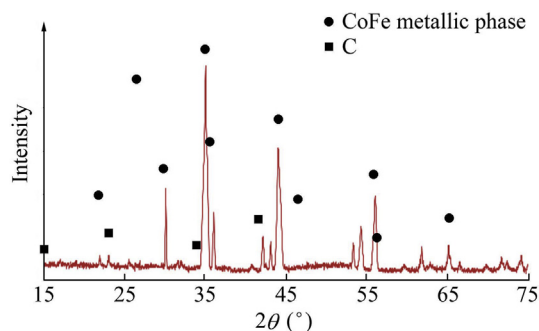

Fig. 3. XRD diffractogram of developed CF-AC.

possesses an incredibly large volume and pores available for the adsorption or ions uptakes. The adsorption of chromium and lead ions were fast after 20 min, and thereafter they gradually reached equilibrium at 80 min. Maximum sorption was obtained at 80 min for Cr(VI) and Pb(II), with Cr reaching a removal efficiency of 92.45%, and Pb(II) showed a removal efficiency of 89.55%. This finding agrees with that of Ali et al. (2019) for chromium and lead removal with a trend of Cr(VI) > Pb(II). Moreover, a further increase in contact time had no significant influence on the removal of both metal ions, probably due to the saturation of the adsorbent surface with Cr and Pb(II). Therefore, the optimum contact time was chosen as 80 min for the process and for further investigation.

3.4. Effect of adsorbent dose

The effect of adsorbent dose on the removal efficiency of the developed CF-AC adsorbents, was examined through experiments with the adsorption of chromium and the lead from tannery wastewater. As shown in Fig. 4(b), the effects of adsorbent dose on the removal efficiencies of heavy metals are paramount in the adsorption processes. It was found that the removal efficiencies of both Cr and Pb(II) ions increase as the adsorbent dose increases. This could be linked to the presence of more active pores on the surfaces of the adsorbents that aid

the adsorption process. The maximum removal efficiencies of 98.9% for Cr and 96.4% for Pb(II) were obtained at 0.8 and 1 g of the adsorbent, respectively. In addition, a further increase of adsorbent dose was found to have no significant impact on the removal of both ions. Sari et al. (2007) observed that metal ions compete for limiting adsorption sites at a low dose. Therefore, 0.8 g was chosen as the optimum adsorbent dose for further investigation.

3.5. Effect of pH of solution

The effect of pH was investigated at a pH range of 2−7 at optimum contact time, using the optimum dose of adsorbent. The initial pH of a solution is an important parameter that determines the adsorption capacity of an adsorbent for metal ion removal from solution, which usually increases with the increased pH value. The pH of a solution usually affects the degree of ionization of the adsorbate and the surface properties of the adsorbent (Emam et al., 2016). Fig. 4(c) highlights the effect of pH on adsorption of Pb(II) and Cr ions onto $CoFe_2O_4$-AC adsorbent. The equilibrium adsorption activity increased with the increase in pH and reached the maximum removal efficiencies for Cr and Pb(II) at 98.2% and 95.5%, respectively, at a pH value of 5. At pH values higher than 5, adsorption activity decreased. This may be attributed to the
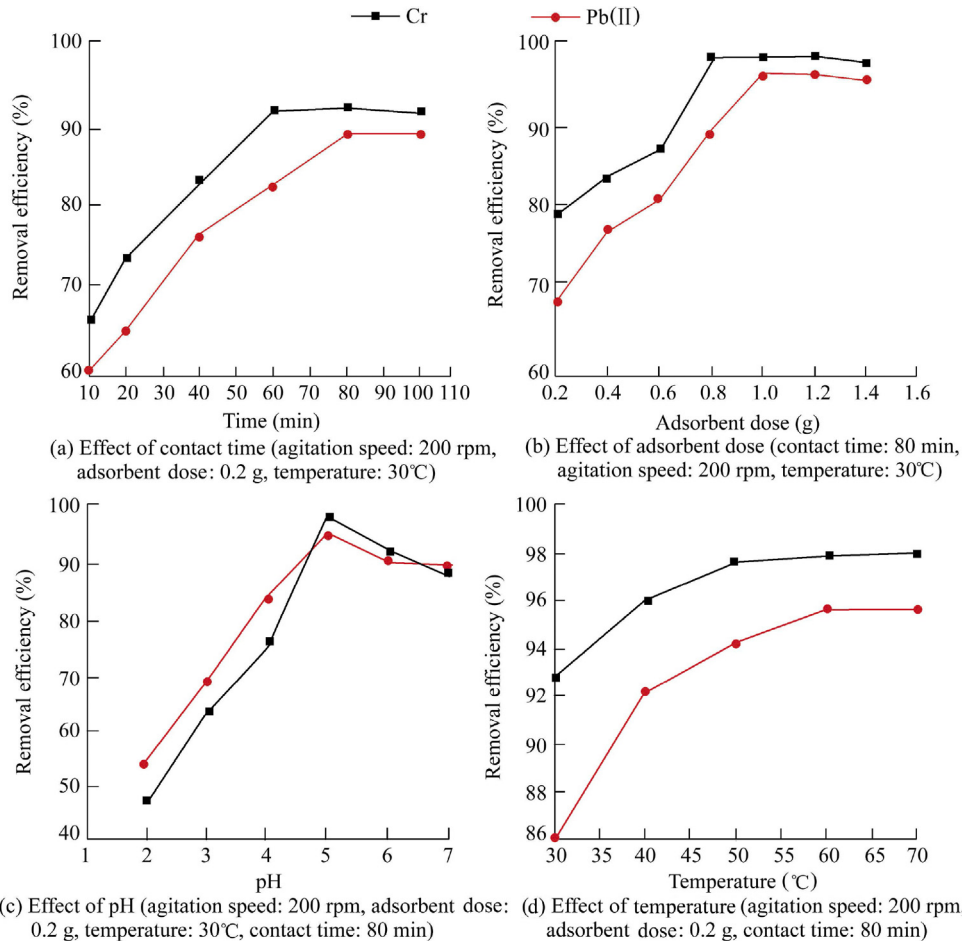

Fig. 4. Effects of contact time, adsorbent dose, pH, and temperature on removal efficiencies of Cr and Pb(II) ions.

diminution of free ions triggered by the formation of hydroxyl complexes at a higher pH range, as reported by Ali et al. (2019). Subsequent precipitation of metal ions in the removal efficiency was observed to decrease. Therefore, as pH of solution increases, the number of protons available for competition decreases. This is a result of the active sites becoming neutral and/or more negatively charged. However, the sorption of the positively charged metal ions is increased via electrostatic force of attraction.

3.6. Effect of temperature

The effect of temperature on the removal efficiencies of chromium and lead from tannery wastewater was examined by varying the temperature of the adsorption process from the room temperature of 30°C−70°C in a batch sorption process. Fig. 4(d) shows the effect of temperature on the removal efficiencies of lead and chromium from tannery wastewater. The results indicate that the removal efficiency of Cr increases from 92.82% at 30°C to 98.03% up to a maximum point of 60°C. Furthermore, after reaching equilibrium, no further increase in the removal efficiency was found as the temperature increased. The removal efficiency of Pb(II) increased gradually from 85.98% at 30°C to 95.69% at 60°C, and after that, no further increase in the removal efficiency was observed. From the obtained results, temperature increase enhances the mobility of Cr and Pb(II) ions and decreases the retarding force that acts on the diffusing ions. This results in the enhancement of the sorptive capacity of the adsorbent, increase of chemical interaction between adsorbate and adsorbent, and generation of active surface centers on an enhanced rate of intraparticle diffusion of Cr and Pb(II) ions into the pores of adsorbent at higher temperature (Bouhamed et al., 2012). This also shows that the adsorption of chromium and lead are endothermic in nature. The effects of operating conditions, such as contact time, adsorbent dose, pH, and temperature were examined through the removal efficiencies of chromium and lead ions from the tannery wastewater, using the batch adsorption process.

3.7. Adsorption isotherm

The linearized form of the Langmuir model equation is as follows:

$$\frac{C_e}{q_e} = \frac{1}{q_{max}K_L} + \frac{C_e}{q_{max}} \tag{3}$$

where q_{max} is the maximum monolayer adsorption capacity (mg/g), and K_L is the Langmuir constant (L/mg) for the monolayer adsorption capacity and affinity of adsorbent towards the adsorbate. The graph of C_e/q_e is plotted against C_e. To affirm the fitness of the Langmuir model to the experimental data, an equilibrium parameter expressed as a dimensionless constant R_L was evaluated. The outcome of R_L values obtained is interpreted as follows: the adsorption system with $R_L > 1$, $0 < R_L < 1$, $R_L = 1$, and $R_L = 0$ is unfavorable, favorable, linear, and irreversible, respectively.

The dimensionless separation factor R_L is given by the following equation:

$$R_L = \frac{1}{1 + K_L C_0} \tag{4}$$

where C_0 is the initial concentration of the metal ions (mg/g).

The linear form of the Freundlich isotherm model equation is given by the following equation:

$$\lg q_e = \lg K_F + \frac{1}{n} \lg C_e \tag{5}$$

where K_F (L/g) and n are the Freundlich equilibrium coefficients. The graph of $\lg q_e$ is plotted against $\lg C_e$, the value of n gives information about favorability of the adsorption process, and K_F is the adsorption capacity of the adsorption.

The Temkin linear form of the equation is as follows:

$$q_e = B \ln A_T + B \ln C_e \tag{6}$$

where the Temkin constant A_T is the equilibrium binding constant corresponding to the maximum binding energy (L/mg).

$$B = \frac{RT}{b_T} \tag{7}$$

where b_T is the heat of adsorption (kJ/mol), R is the universal gas constant (8.314 J/(mol·K)), and T is the temperature in Kelvin (K). The graph of q_e is plotted against $\ln C_e$ at various temperatures.

The Dubinin-Radushkevich (D-R) isotherm model helps to determine the type of adsorption process, whether chemisorption or physisorption. The linearized form is as follows:

$$\ln q_e = \ln q_s - K\varepsilon^2 \tag{8}$$

where q_s is the saturation adsorption capacity (mg/g), K is the activity constant coefficient related to adsorption capacity, and ε is the Polanyi potential (kJ/mol).

The Polanyi potential is estimated using the following equation:

$$\varepsilon = RT \ln\left(1 + \frac{1}{C_e}\right) \tag{9}$$

The graph of $\ln q_e$ was plotted against ε^2. The average energy adsorption E (kJ/mol) is estimated as

$$E = \frac{1}{\sqrt{2K}} \tag{10}$$

According to the Langmuir model, adsorption usually occurs uniformly on the active site of the adsorbent. Once the site is occupied, no further adsorption occurs. The main feature of the Langmuir isotherm can be expressed by R_L. However, a lower R_L value suggests that adsorption is more favorable, indicated by $0 < R_L < 1$, whereas an R_L value greater than one means that the adsorption nature is unfavorable, indicated by $R_L > 1$, linearity is indicated by $R_L = 1$, and irreversibility is indicated by $R_L = 0$. From the obtained

results, R_L is greater than 0 but less than 1, indicating that the Langmuir isotherm is favorable. From this work, the maximum monolayer coverage capacity (Q_m) from the Langmuir isotherm model and the K_L values were determined to be 23.6 mg/g and 0.191 2 L/mg for Cr, and 6.27 mg/g and 0.133 5 L/mg for Pb(II), respectively. The R_L values were 0.393 (for Cr) and 0.473 (for Pb(II)), indicating that the equilibrium sorption was favorable. However, the coefficient of determination (R^2) values of 0.813 (for Cr) and 0.747 (for Pb(II)) were not close to one. Therefore, they did not represent strong model applicability (Nethaji et al., 2013).

According to Dawodu et al. (2012), the Freundlich isotherm was developed for a heterogeneous surface, and it involves a multilayer adsorption on the sorbent surface. The R^2 values recorded for chromium and lead ions were 0.948 and 0.932, respectively. It proves that the sorption data were well fitted to this model. Also, the results from this work show the value of $1/n$, which represents the Freundlich coefficient, was less than 1. With a smaller $1/n$, the expected heterogeneity was greater. The $1/n$ values obtained for Cr and Pb(II) were 0.665 and 0.135, respectively. This implies a favorable adsorption because the value is low and falls within the range ($0.1 < 1/n < 1$) (Desta, 2013). However, the best fit of the Freundlich isotherm model shows favourable adsorption of Cr and Pb(II) onto the adsorbent heterogeneity surface, which was observed from the value condition of $0 < 1/n < 1$ satisfying the favourability and heterogeneity of the model.

The Temkin adsorption isotherm was considered in adsorbent-adsorbate interactions. The obtained R^2 values were 0.937 and 0.937 for Cr and Pb(II) ions, respectively. It can be deduced that Cr has a better applicability than Pb(II). Dada et al. (2012) stated that high values of b_T indicate strong interaction between metal ions and adsorbent. From the obtained results, the constant b_T was 1.46 kJ/mol for Cr and 2.48 kJ/mol for Pb(II). This constant indicates a weak interaction between metal ions and adsorbent. Consequently, this model does not fit well to this study.

This is a model that is effectively applied for adsorption of heterogeneous systems, including solids and liquids (Hameed and Foo, 2010). From the linear plot of the D-R isotherm model, the q_s values were determined to be 42.99 mg/g for Cr and 168.20 mg/g for Pb(II). The E values were 0.408 and 0.316 kJ/mol for Cr and Pb(II), respectively. The value of E lower than 8 kJ/mol indicates physical adsorption, whereas an E value higher than 8 kJ/mol demonstrates chemical adsorption. The obtained E values for both adsorbed metals reveal that the adsorption mechanism is physical ($E < 8$ kJ/mol). Table 5 shows comparison of monolayer adsorption capacity of Cr and Pb(II) onto various adsorbents.

3.8. Adsorption kinetic studies

The study of adsorption kinetics describes the solute uptake rate. Evidently, this rate controls the residence time of adsorbate uptake at the solid-solution interface. Taha et al. (2018) reported that a kinetic model helps in the study of adsorption rates, models the process, and predicts information about adsorbent/adsorbate interaction (physisorption or chemisorption). The kinetics of Cr and Pb(II) adsorption onto CF-AC were determined using pseudo-first order, pseudo-second order, Elovich, and intraparticle kinetic models.

The linear form of the pseudo-first order kinetic model is as follows.

$$\lg (q_e - q_t) = \lg q_e - \frac{k_1}{2.303} t \tag{11}$$

where k_1 is the first order rate constant (min^{-1}) obtained from the plot of $\lg (q_e - q_t)$ against the adsorption time t (min), and q_t (mg/g) is the amount of metal ions adsorbed at t.

The linear form of the pseudo-second order kinetic model equation is as follows:

$$\frac{t}{q_t} = \frac{1}{k_2 q_e^2} + \frac{t}{q_e} \tag{12}$$

where k_2 (g/(mg·min)) is the pseudo-second order rate constant.

The Elovich model is widely employed to describe the sorbate adsorption from solution onto the surfaces, as well as the pores of adsorbents. The Elovich model's linear equation form is as follows:

$$q_t = \frac{1}{\beta_e} \ln (\alpha \beta_e) - \frac{1}{\beta_e} \ln t \tag{13}$$

where α and β_e are Elovich constants, which are obtained from the plots of q_t against $\ln t$.

Mechanisms of Cr and Pb(II) adsorption were investigated by testing the possibility of intraparticle diffusion as a rate-limiting step using the intraparticle diffusion model, which can be represented as follows:

$$q_t = k_i t^{0.5} + C \tag{14}$$

where k_i is the intraparticle rate constant (mg/(g·min$^{0.5}$)), and C is the plot intercept. The graph of q_t was plotted against $t^{0.5}$. Bello et al. (2010) found that the rate adsorption constant was determined from the first-order equation given by Lagergren and Svenska (1898). The R^2 values were determined to be 0.200 and 0.164 for Cr and Pb(II), respectively. The low R^2

Table 5
Comparison of uptake capacity of Cr and Pb(II) on various adsorbents.

Adsorbent	Metal uptake capacity (mg/g)		Reference
	Cr	Pb(II)	
P-CNTs	3.39		Hamzat et al. (2019)
Dolochar	1.90	2.12	Panda et al. (2011)
Magnetite particle	0.015		Padmavathy et al. (2016)
Polyamide/CNT composite		3.2	Albakri et al. (2018)
CoFe$_2$O$_4$/NOM	5.99		Cruz et al. (2017)
Raw almond shell	21.92		Yahya et al. (2020b)
Cashew nut shell	10.79		Yahya et al. (2020c)
Soy hull	7.29		Blanes et al. (2016)
CF-AC	23.6	6.27	This study

value obtained from the pseudo-first order kinetic model indicates that sorption is not taking place uniformly on the active site of the adsorbent (Nuhoglu and Malkoc, 2009).

The R^2 values for the pseudo-second order model suggested the applicability of the pseudo-second order kinetic model, 0.999 (Cr) and 0.996 (Pb(II)), to describe the adsorption process of Cr and Pb(II) uptake on CF-AC. The plot of t/q_t versus t (figure not shown) shows a good linear relationship as compared to the plot of the pseudo-first order kinetic model. Also, a close agreement between calculated q_e and experimental q_e (0.137 and 0.132, respectively) was recorded for Cr whereas the respective values were 0.038 and 0.039 for Pb(II), indicating that this model is suitable to describe the rate of Cr and Pb(II) uptake by the adsorbent. Therefore, the kinetic adsorption could be satisfactory and more favorably described by a pseudo-second order kinetic model for Cr and Pb(II) adsorption onto CF-AC (Ho and McKay, 1999).

The intraparticle model shows a high correlation value, and the R^2 values were 0.907 for Cr and 0.945 for Pb(II). The correlation from the intraparticle model is better than that of the first-order kinetic model. This is because the boundary layer has a more significant effect regarding the diffusion mechanism of Cr and Pb(II) uptake on the adsorbent. If the plot of q_e versus $t^{0.5}$ yields a straight line passing through the origin, then the adsorption process is only controlled by intraparticle diffusion. However, if the data show multi-linear plots, then two or more steps are influencing the adsorption processes. The plots of Cr and Pb(II) deviate from the origin. This indicates that intraparticle diffusion is not the only rate-determining factor (Obayomi et al., 2019). The R^2 values for the Elovich model were determined to be 0.990 (Cr) and 0.988 (Pb(II)). These values were close to those of the pseudo-second order kinetic model. This result basically agrees with that of previous studies, which found that the Elovich model relates to the pseudo-second order kinetic model by assuming sorbent heterogeneity. The equation is often valid for systems in which the adsorbing surface is heterogeneous (Namasivayam and Kavitha, 2009). In reactions involving chemisorption of adsorbate on a solid surface without desorption of products, the adsorption rate decreases with time, due to an increased surface coverage (Ali et al., 2016).

3.9. Model applicability test for isotherm model

The prediction of best fit model was based on:

(1) Precision testing comparing $q_{e,cal}$ and $q_{e,exp}$, which are the calculated adsorbate concentration at equilibrium (mg/g) and the experimental adsorbate concentration at equilibrium (mg/g), respectively.

(2) Regression analysis using the R^2 applicability test.

(3) The sum of square error (E_s):

$$E_s = \sum_{i=1}^{N} \left(q_{ei,cal} - q_{ei,exp} \right)^2 \tag{15}$$

$$E_h = \frac{100}{N-p} \sum_{i=1}^{N} \left(\frac{q_{ei,exp} - q_{ei,cal}}{q_{ei,exp}} \right) \tag{16}$$

where E_h is the hybrid fractional error function; N is the number of data points; $q_{ei,cal}$ and $q_{ei,exp}$ are the ith calculated and experimental adsorbate concentrations at equilibrium, respectively; and p is the number of parameters (Demirbas et al., 2008; Rostamian et al., 2011).

Error analysis was conducted to check the fitness of the adsorption model to experimental data, and error functions were used by Rostamian et al. (2011). In this work, two error functions were used on the linear form of data by minimizing the error functions within a range of concentration. Table 6 presents the error functions for optimization of equilibrium isotherms. Through comparing the results of the values for the error functions and R^2, it was found that the Freundlich isotherm generally represents the equilibrium sorption with low value for the error function.

The error analysis for equilibrium isotherms follows the sequence below: for R^2, Freundlich > Temkin > Dubinin-Radushkevich > Langmuir; for E_s, Dubinin-Radushkevich > Langmuir > Temkin > Freundlich; and for E_h, Temkin > Dubinin-Radushkevich > Langmuir > Freundlich.

3.10. Adsorption thermodynamics

The change in the Gibbs free energy (ΔG), the change in the enthalpy (ΔH), and the change in the entropy (ΔS) of the adsorption system were evaluated to determine the thermodynamic parameters of the adsorption system. The thermodynamic mathematical expression is given below:

$$\ln K_c = \frac{\Delta S}{R} - \frac{\Delta H}{RT} \tag{17}$$

$$\Delta G = -RT \ln K_c \tag{18}$$

where K_c represents the equilibrium constant. The data were fitted to generate the enthalpy, Gibbs free energy, and entropy of the adsorption process, for the respective adsorbents.

The thermodynamic parameter changes ΔG, ΔH, and ΔS, for the adsorption of Cr and Pb(II) ions onto CF-AC, were determined using Eqs. (17) and (18). Adsorption of Cr and Pb(II) onto CF-AC was found to increase with temperature increase. Table 7 presents the parameter thermodynamic values. The slop and intercept provided values of ΔH and ΔS, respectively. ΔG showed a negative value in all temperature

Table 6
Error analysis studies for isotherm model.

Isotherm	R^2		E_s		E_h	
	Cr	Pb(II)	Cr	Pb(II)	Cr	Pb(II)
Freundlich	0.948 4	0.912 0	0.001 9	0.000 6	0.004 7	0.001 6
Langmuir	0.812 5	0.746 8	0.027 0	0.003 2	0.889 0	0.041 9
Temkin	0.937 1	0.936 7	0.066 7	0.000 7	5.416 4	0.002 1
Dubinin-Radushkevich	0.894 3	0.850 1	0.023 5	0.007 71	0.671 3	0.250 6

Table 7
Thermodynamic adsorption values for Cr and Pb(II) adsorption onto CF-AC.

Adsorbate	ΔH (kJ/mol)	ΔS (J/(mol·K))	ΔG (kJ/mol)					R^2
			298 K	313 K	323 K	333 K	343 K	
Cr	27.442	108.560	−4.627	−6.566	−8.229	−8.891	−9.248	0.924
Pb(II)	24.987	94.920	−2.775	−4.638	−5.674	−6.664	−6.840	0.694

ranges. These negative values represent the spontaneous nature as well as the feasibility of adsorption reaction (Singha and Das, 2011). A decrease in ΔG with temperature increase shows better sorption at increased temperature. The positive value of enthalpy changes for both metals revealed the endothermic nature of the adsorption process. The positive entropy values indicate that there is randomness during the adsorbate-adsorbent interaction in the adsorption process. The absolute value of Gibbs free energy from −20 to 0 kJ/mol shows that physical adsorption is from −20 to 0 kJ/mol whereas values ranging from −80 to −400 kJ/mol are for chemical adsorption. The Gibbs free energy obtained in this study further affirmed that the adsorption processes for both metals were physical in nature.

4. Conclusions

The application of the situ method of CF-AC resulted in the formation of an improved adsorbent capable of removing a higher percentage of pollutants from the tannery waste-water. The characterization results revealed that the CF-AC produced from almond husks were composed of organic and mineral matters that have variety of functional groups. These functional groups play a vital role in the adsorption process. The adsorption studies of pH of solution, contact time, temperature, and adsorbent dose were found to have effects on the uptake. Furthermore, Cr and Pb(II) ions were most effectively adsorbed at a pH value of 5. The adsorption of metal ions on CF-AC attained equilibrium within 80 min. The maximum adsorbed amount of Cr and Pb(II) ions were 23.6 and 6.27 mg/g, respectively. The adsorption kinetic model revealed that the pseudo-second order model well described the adsorption of Cr and Pb(II) onto CF-AC, and the Freundlich model was seen to best fit to the adsorption data for both metals. The thermodynamic parameter analysis revealed the adsorption of Cr and Pb(II) by CF-AC as spontaneous, endothermic, and physical in nature. The developed CF-AC can be used to effectively salvage pollution problems posed by both Cr and Pb(II) ions in the environment.

Declaration of competing interest

The authors declare no conflicts of interest.

References

Ahalya, N., Ramachandra, T.V., Kanamadi, R., 2003. Biosorption of heavy metals. Res. J. Chem. Environ. 7(4), 71−79.

Albakri, M.A., Abdelnaby, M.M., Saleh, T.A., Al Hamouz, O.C.S., 2018. New series of benzene-1,3,5-triamine based cross-linked polyamines and polyamine/CNT composites for lead ion removal from aqueous solutions. Chem. Eng. J. 333, 76−84. https://doi.org/10.1016/j.cej.2017.09.152.

Ali, I.H., Al Mesfer, M.K., Khan, M.I., Danish, M., Alghamdi, M.M., 2019. Exploring adsorption process of lead(II) and chromium(VI) ions from aqueous solutions on acid activated carbon prepared from *Juniperus procera* leaves. Processes 7(4), 217. https://doi.org/10.3390/pr7040217.

Ali, R.M., Hamada, H.A., Hussein, M.M., Malash, G.F., 2016. Potential of using green adsorbent of heavy metal removal from aqueous solutions: Adsorption kinetics, isotherm, thermodynamic, mechanism and economic analysis. Ecol. Eng. 91, 317−332. https://doi.org/10.1016/j.ecoleng.2016.03.015.

Amarasinghe, B.M.W.P.K., Williams, R.A., 2007. Tea waste as a low cost adsorbent for the removal of Cu and Pb from wastewater. Chem. Eng. J. 132(1−2), 299−309. https://doi.org/10.1016/j.cej.2007.01.016.

Bello, O.S., Adelaide, O.M., Abdul Hammed, M., Abdul Muiz Popoola, O., 2010. Kinetic and equilibrium studies of methylene blue removal from aqueous solution by adsorption on treated sawdust. Macedon. J. Chem. Chem. Eng. 29(1), 77−85. https://doi.org/10.20450/mjcce.2010.181.

Bhatnagar, A., Sillanpaa, M., Witek-Krowiak, A., 2015. Agricultural waste peels as versatile biomass for water purification: A review. Chem. Eng. J. 270, 244−271. https://doi.org/10.1016/j.cej.2015.01.135.

Blanes, P.S., Bordoni, M.E., Gonzáleza, J.C., Garcíaa, S.I., Atriac, A.M., Sala, L.F., Bellú, S.E., 2016. Application of soyhull biomass in removal of Cr(VI) from contaminated waters: Kinetic, thermodynamic and continuous sorption studies. J. Environ. Chem. Eng. 4(1), 516−526. https://doi.org/10.1016/j.jece.2015.12.008.

Bouhamed, F., Elouear, Z., Bouzid, J., 2012. Adsorptive removal of copper(II) from aqueous solutions on activated carbon prepared from Tunisian date stones: Equilibrium, kinetics and thermodynamics. J. Taiwan Instit. Chem. Eng. 43(5), 741−749. https://doi.org/10.1016/j.jtice.2012.02.011.

Chukwu, U.J., John, E.P., Kalagbor, A.I., 2017. Adsorption of Cu^{2+} and Fe^{2+} from single metal ion solution using unmodified and formaldehyde modified kola-nut (*Cola nitida*) testa. IOSR J. Appl. Chem. 10(12), 12−18. https://doi.org/10.9790/5736-1012011218.

Coskun, R., Savci, S., Delibas, A., 2018. Adsorption properties of activated almond shells for methylene blue. Environ. Res. Tehnol. 1(2), 31−38.

Cotica, L.F., Freitas, V.F., Silva, D.M., Honjoya, K., Honjoya, K., Santos, I.A., Fontanive, V.C.P., Khalil, N.M., Mainardes, R.M., Kioshima, E.S., et al., 2014. Thermal decomposition synthesis and assessment of effect on blood cells *in vivo* damages of cobalt ferrite nanoparticles. J. Nano Res. 28, 131−140. https://doi.org/10.4028/www.scientific.net/JNanoR.28.131.

Cruz, D.R.S., Santos, B.T.J., Cunha, G.C., Romao, L.P.C., 2017. Green synthesis of a magnetic hybrid adsorbent ($CoFe_2O_4$/NOM): Removal of chromium from industrial effluent and evaluation of the catalytic potential of recovered chromium ions. J. Hazard Mater. 334, 76−85. https://doi.org/10.1016/j.jhazmat.2017.03.062.

Czikkely, M., Neubauer, E., Fekete, I., Ymeri, P., Fogarassy, C., 2018. Review of heavy metal adsorption processes by several organic matters from wastewaters. Water 10(10), 1377. https://doi.org/10.3390/w10101377.

Dada, A.O., Olalekan, A.P., Olatunya, A.M., Dada, O., 2012. Langmuir, Freundlich, Temkin and Dubinin-Radushkevich isotherms studies of equilibrium sorption of Zn^{2+} unto phosphoric acid modified rice husk. IOSR J. Appl. Chem. 3(1), 38−45. https://doi.org/10.9790/5736-0313845.

Dawodu, F.A., Akpomie, G.K., Abuh, M.A., 2012. Batch sorption of lead(II) from aqueous stream by "Eluku" clay-equilibrium, kinetic and thermodynamic studies. Int. J. Multidiscip. Sci. Eng. 3(10), 32−37.

Demirbas, E., Kobya, M., Konukman, A.E.S., 2008. Error analysis of equilibrium studies for the almond shell activated carbon adsorption of Cr(VI) from aqueous solutions. J. Hazard Mater. 154(1–3), 787–794. https://doi.org/10.1016/j.jhazmat.2007.10.094.

Desta, M.B., 2013. Batch sorption experiments: Langmuir and Freundlich isotherm studies for the adsorption of textile metal ions onto teff straw (*Eragrostis tef*) agricultural waste. J. Thermodyn. 6(1), 375830. https://doi.org/10.1155/2013/375830.

Ekpete, O.A., Horsfall Jr., M., 2011. Preparation and characterization of activated carbon derived from fluted pumpkin stem waste (*Telfairia occidentalis Hook F*). Res. J. Chem. Sci. 1(3), 10–17.

Emam, A.A., Ismail, L.F.M., AbdelKhalek, M.A., AzzaRezhan, 2016. Adsorption study of some heavy metal ions on modified kaolinite clay. Int. J. Advan. Eng. Technol. Manag. Appl. Sci. 3(7), 152–163.

Haktanır, C., Özbelge, H.O., Bıçak, N., Yılmaz, L., 2017. Removal of hexavalent chromium anions via polymer enhanced ultrafiltration using a fully ionized polyelectrolyte. Separ. Sci. Technol. 52(15), 2487–2497. https://doi.org/10.1080/01496395.2017.1343351.

Hameed, B.H., Foo, K.Y., 2010. Insight into the modeling of adsorption isotherms system. Chem. Eng. J. 156(1), 2–10. https://doi.org/10.1016/j.cej.2009.09.013.

Hamzat, W.A., Abdulkareem, A.S., Bankole, M.T., Tijani, J.O., Kovo, A.S., Abubakre, O.K., 2019. Adsorption studies on the treatment of battery wastewater by purified carbon nanotubes (P-CNTs) and polyethylene glycol carbon nanotubes (PEG-CNTs). J. Environ. Sci. Health, A 54(9), 827–839. https://doi.org/10.1080/10934529.2019.1596701.

Ho, Y.S., McKay, G., 1999. Pseudo-second order model for sorption processes. Process Biochem. 34(5), 735–742. https://doi.org/10.1016/S0032-9592(98)00112-5.

Huang, D.D., Wang, G.C., Shi, Z.M., Li, Z.H., Kang, F., Liu, F., 2017. Removal of hexavalent chromium in natural groundwater using activated carbon and cast iron combined system. J. Clean. Prod. 165, 667–676. https://doi.org/10.1016/j.jclepro.2017.07.152.

Joshi, S., Pokharel, B.P., 2014. Preparation and characterization of activated carbon from Lapsi (*Choerospondias axillaris*) seed stone by chemical activation with potassium hydroxide. J. Inst. Eng. 9(1), 79–88. https://doi.org/10.3126/jie.v9i1.10673.

Kothai, P., Meena, A., Meenaloshini, E., Revathy, A., Kumar, N.V., 2019. Treatment of tannery effluent using groundnut shells. Int. Res. J. Eng. Technol. 6(3), 2395-0072.

Kurian, M., Thankachan, S., Nair, D.S., Aswathy, E.K., Aswathy, B., Arathy, T., Binu Krishna, K.T., 2015. Structural, magnetic, and acidic properties of cobalt ferrite nanoparticles synthesized by wet chemical methods. J. Adv. Ceram. 4(3), 199–205. https://doi.org/10.1007/s40145-015-0149-x.

Lagergren, S., Svenska, S.K., 1898. On the theory of so-called adsorption of dissolved substances. R. Swed. Acad. Sci. Doc. 24, 1–13.

Lofrano, G., Meric, S., Zengin, G.E., Orhon, D., 2013. Chemical and biological treatment technologies for leather tannery chemicals and wastewaters: A review. Sci. Total Environ. 461–462, 265–281. https://doi.org/10.1016/j.scitotenv.2013.05.004.

Manjuladevi, M., Sri, O.M., 2017. Heavy metals removal from industrial wastewater by nano adsorbent prepared from cucumis melopeel activated carbon. J. Nanomed. 5(1), 00102. https://doi.org/10.15406/jnmr.2017.05.00102.

Mierzwa-Hersztek, M., Gondek, K., Jewiarz, M., Dziedzic, K., 2019. Assessment of energy parameters of biomass and biochars, leachability of heavy metals and phytotoxicity of their ashes. J. Mater. Cycles Waste Manag. 21, 786–800. https://doi.org/10.1007/s10163-019-00832-6.

Namasivayam, C., Kavitha, D., 2009. Removal of Congo red from water by adsorption on activated carbon prepared from coir pith, an agricultural waste. Dyes Pigments 54(1), 47–58. https://doi.org/10.1016/S0143-7208(02)00025-6.

Nasseh, N., Taghavi, L., Barikbin, B., Harifi-Mood, A.R., 2016. The removal of Cr(VI) from aqueous solution by almond green hull waste material: Inetic and equilibrium studies. J. Water Reuse Desalin. 7(4), 449–460. https://doi.org/10.2166/wrd.2016.047.

Nethaji, S., Sivasamy, A., Mandal, A.B., 2013. Adsorption isotherms, kinetics and mechanisms for the adsorption of cationic and anionic dyes onto carbonaceous particles prepared from *Juglans regia* shell biomass. Int. J. Sci. Technol. 10, 231–242. https://doi.org/10.1007/s13762-012-0112-0.

Nuhoglu, Y., Malkoc, E., 2009. Thermodynamic and kinetic studies for environmental friendly Ni(II) biosorption using waste pumice of olive oil. J. Biores. Technol. 100(8), 2375–2380. https://doi.org/10.1016/j.biortech.2008.11.016.

Obayomi, K.S., Auta, M., 2019. Development of microporous activated Aloji clay for adsorption of lead(II) from aqueous solution. Heliyon 5(11), e02799. https://doi.org/10.1016/j.heliyon.2019.e02799.

Obayomi, K.S., Bello, J.O., Nnoruka, J.S., Adediran, A.A., Olajide, P.O., 2019. Development of low-cost bio-adsorbent from agricultural waste composite for Pb(II) and As(III) sorption from aqueous solution. Cogent Eng. 6(1), 1687274. https://doi.org/10.1080/23311916.2019.1687274.

Obayomi, K.S., Auta, M., Kovo, A.S., 2020. Isotherm, kinetic and thermodynamics studies for adsorption of lead(II) onto modified Aloji clay. Desalinat. Water Treat. 181, 376–384. https://doi.org/10.5004/dwt.2020.25142.

Padmavathy, K.S., Madhub, G., Haseena, P.V., 2016. A study on effects of pH, adsorbent dosage, time, initial concentration and adsorption isotherm study for the removal of hexavalent chromium (Cr(VI)) from wastewater by magnetite nanoparticles. Procedia Technol. 24, 585–594. https://doi.org/10.1016/j.protcy.2016.05.127.

Panda, L., Das, B., Rao, D.S., Mishra, B.K., 2011. Application of Dolochar in the removal of cadmium and hexavalent chromium ions from aqueous solutions. J. Hazard Mater. 192(2), 822–831. https://doi.org/10.1016/j.jhazmat.2011.05.098.

Rostamian, R., Najafi, M., Rafati, A.A., 2011. Synthesis and characterization of thiol-functionalized silica nano hollow sphere as a novel adsorbent for removal of poisonous heavy metal ions from water: Kinetics, isotherms and error analysis. Chem. Eng. J. 171(3), 1004–1011. https://doi.org/10.1016/j.cej.2011.04.051.

Saranya, K., Thirumarimurugan, M., Manivasagan, V., 2016. Biosorption of hexavalent chromium from paint industrial effluent by *Saraca indica* leaves using with and without gel entrapment method. Int. J. Environ. Sustain. Dev. 15(3), 219–226. https://doi.org/10.1504/IJESD.2016.077365.

Sari, A., Tuzen, M., Soylak, M., 2007. Adsorption of Pb(II) and Cr(III) from aqueous solution on Celtek clay. J. Hazard Mater. B 144(1–2), 41–46. https://doi.org/10.1016/j.jhazmat.2006.09.080.

Sharma, K.P., Ayub, S., Tripathi, C.N., 2013. Agro and horticultural wastes as low cost adsorbents for removal of heavy metal from wastewater: A review. Int. Ref. J. Eng. Sci. 2(8), 18–27.

Singh, D.K., Kumar, V., Mohan, S., Bano, D., Hasan, S.H., 2017. Breakthrough curve modeling of graphene oxide aerogel packed fixed bed column for the removal of Cr(VI) from water. J. Water Process Eng. 18, 150–158. https://doi.org/10.1016/j.jwpe.2017.06.011.

Singha, B., Das, S.K., 2011. Biosorption of Cr(VI) ions from aqueous solutions: kinetics, equilibrium, thermodynamics and desorption studies. Colloids Surf. B Biointerfaces 84(1), 221–232. https://doi.org/10.1016/j.colsurfb.2011.01.004.

Song, M., Jin, B.S., Xiao, R., Yang, L., Wu, Y.M., Zhong, Z.P., Huang, Y.J., 2013. The comparison of two activation techniques to prepare activated carbon from corn cob. Biomass Bioenergy 48, 250–256. https://doi.org/10.1016/j.biombioe.2012.11.007.

Sonja, J., Ksenija, K., Danica, B.B., Bostjan, J., Matjaz, S., Tatjanai, T.P., Danilo, S., 2019. Cobalt ferrite nanospheres as a potential magnetic adsorbent for chromium(VI) ions. J. Nanosci. Nanotechnol. 19(8), 5027–5034. https://doi.org/10.1166/jnn.2019.16803.

Srivastava, V.C., Swamy, M.M., Mall, I.D., Prasad, B., Mishra, I.M., 2010. Adsorptive removal of phenol by Bagasse fly ash and activated carbon: Equilibrium, kinetics and thermodynamics. Colloid. Surface. Physicochem. Eng. Aspect. 272(1–2), 89–104. https://doi.org/10.1016/j.colsurfa.2005.07.016.

Swathi, M., Sathya, S.A., Aravind, S., Ashi-Sudhakar, P.K., Gobinath, R., Saranya, D., 2014. Adsorption studies on tannery wastewater using rice

husk. Scholars J. Eng. Technol. 2(2B), 253−257. https://doi.org/10.36347/sjet.

Taha, A., Moustafa, A.H.E., Abdel-Rahman, H., Abd-El-Hameed, M.A., 2018. Comparative biosorption study of Hg(II) using raw and chemically activated almond shell. Adsorpt. Sci. Technol. 36(1−2), 521−548. https://doi.org/10.1177/0263617417705473.

Vazquez-Olmos, A.R., Abatal, M., Sato-Berru, R.Y., Pedraza-Basulto, G.K., Garcia-Vazquez, V., Sainz-Vidal, A., Perez-Bañuelos, R., Quiroz, A., 2016. Mechanosynthesis of MFe$_2$O$_4$ (M=Co, Ni, and Zn) magnetic nanoparticles for Pb removal from aqueous solution. J. Nanomater. 2016, 9182024. https://doi.org/10.1155/2016/9182024.

Veit, M.T., Tavares, C.R.G., Gomes-da-Costa, S.M., Guedes, T.A., 2005. Adsorption isotherms of copper(II) for two species of dead fungi biomass process. Biochemistry 40(10), 3303−3308. https://doi.org/10.1016/j.procbio.2005.03.029.

Wambu, E.W., Attahiru, S., Shiundu, P.M., Wabomba, J., 2018. Removal of heavy-metals from wastewater using a hydrous alumino-silicate mineral from Kenya. Bull. Chem. Soc. Ethiop. 32(1), 39−51. https://doi.org/10.4314/bcse.v32i1.4.

Yahya, M.D., Yohanna, I., Auta, M., Obayomi, K.S., 2020a. Remediation of Pb(II) ions from Kagara gold mining effluent using cotton hull adsorbent. Sci. African 8, e00399. https://doi.org/10.1016/j.sciaf.2020.e00399.

Yahya, M.D., Abubakar, H., Obayomi, K.S., Iyaka, Y.A., Suleiman, B., 2020b. Simultaneous and continuous biosorption of Cr and Cu(II) ions from industry tannery effluent using almond shell in a fixed bed column. Res. Eng. 6, 100113. https://doi.org/10.1016/j.rineng.2020.100113.

Yahya, M.D., Aliyu, A.S., Obayomi, K.S., Olugbenga, A.G., Abdullahi, U.B., 2020c. Column adsorption study for the removal of chromium and manganese ions from electroplating water using cashew nutshell adsorbent. Cogent Eng. 7(1), 1748470. https://doi.org/10.1080/23311916.2020.1748470.

Yahya, N., Kashif, M., Nasir, N., Niaz Akhtar, M., Yusof, N.M., 2012. Cobalt ferrite nanoparticles: An innovative approach for enhanced oil recovery application. J. Nano Res. 17, 115−126. https://doi.org/10.4028/www.scientific.net/JNanoR.17.115.

Yakubu, I.S., Muhammad, A.R., Lawan, U., 2018. Determination of heavy metals in tannery effluent. Int. J. Adv. Acad. Res. Sci. Technol. Res. 4(5), 132−134.